Supplementary Materials: "Rubbertown Next Generation Emissions Measurements Demonstration Project"; E. Thoma, I. George, R. Duvall, T. Wu, D. Whitaker , K. Oliver , S. Mukerjee, H. Brantley, J. Spann, T. Bell, N. Carlton-Carew, P. Deshmukh, J. Cansler, T. Cousett, W. Tang, A. Cooley, K. Zimmerman, B. DeWitt, and B. Paris

Supplementary Materials (SM) Tables, Figures, and Videos Page

*Supplementary video descriptions are contained here with the videos included as separate files.

Table SM1: Site and deployment details.

Site Num.	Location Description / Address	Latitude / Longitude	Equip. Deployed	Height AGL (m)	Start Date (mm/dd/yy)	Stop Date (mm/dd/yy)
S1	LMAPCD Firearms Training Center Air Monitoring Site, 4201 Algonquin Pkwy., Louisville, KY 40211	38.231585° / - 85.826808°	S1 PS, SPod FS, MiTAP GC, LMAPCD GC, 10 m Wind	3.5 3.5 1.5 m 3.5 m 10 m	9/12/17 9/13/17* 9/12/17* 11/1/17* 2/13/19*	9/12/18 Ongoing 7/15/18 Ongoing Ongoing
S2	MSD MFWTP / 4300 Gibson Ln., Louisville, KY, 40211	38.228864° / - 85.832658°	S2 PS	1.5 m	9/12/17	9/12/18
S3	MSD MFWTP / 4300 Gibson Ln,. Louisville, KY, 40211	38.230430° / - 85.837547°	S3 PS	1.5 m	9/12/17	9/12/18
S4	Carter Elementary School, 3600 Bohne Ave., Louisville, KY, 40211	38.227325° / - 85.815352°	S4 PS	3.8	9/12/17	9/12/18
S5	MSD Pump Station / 4002 Bells Ln., Louisville, KY, 40211	38.221226° / - 85.823383°	S5 PS	2.0	9/12/17	9/12/18
S6	Cane Run Elementary 3951 Cane Run Rd., Louisville, KY, 40211	38.209153° / - 85.821435°	S6 PS	3.8	9/12/17	9/12/18
S7	4211 Camp Ground Rd., Louisville, KY, 40216	38.211175° / - 85.840637°	S7 PS	1.5	9/13/17	9/12/18
S8	4319 Camp Ground Rd., Louisville, KY, 40216	38.209666° / - 85.842509°	S8 PS, SPod FS, MiTAP GC	2.3	9/13/17* 6/4/18* 7/25/18*	9/13/18 Ongoing Ongoing
S9	MSD Sign, 4300 Senn Rd., Louisville, KY, 40216.	38.208319° / - 85.855805°	S9 PS	2.6	9/13/17	9/12/18
S10	Lake Dreamland Fire Dept., 4912 Camp Ground Rd., Louisville, KY, 40216	38.204611° / - 85.852448°	S10 PS	3.9	9/13/17	9/12/18
S11	Foster Academy, South 41st Street, Louisville, KY 40211	38.236253° / - 85.820429°	S11 PS	3.9	6/19/18	9/12/18

Table SM1. Site and deployment description and dates for the first year of this project. GPS coordinates indicate position of PS (± 2 m) with other equipment within ± 4 m. S2 and S3 were sited on the City of Louisville Metropolitan Sewer District (MSD), Morris Forman Wastewater Treatment Plant (MFWTP) property. Deployment date "ongoing" indicates continuation after first year of study. S8 passive sampler was moved 7 m to SE to stated coordinates on 6/06/18. (*) indicates deployment start but only select data are available due to equipment issues (detailed in future publications).

Figure SM1: Area wind roses

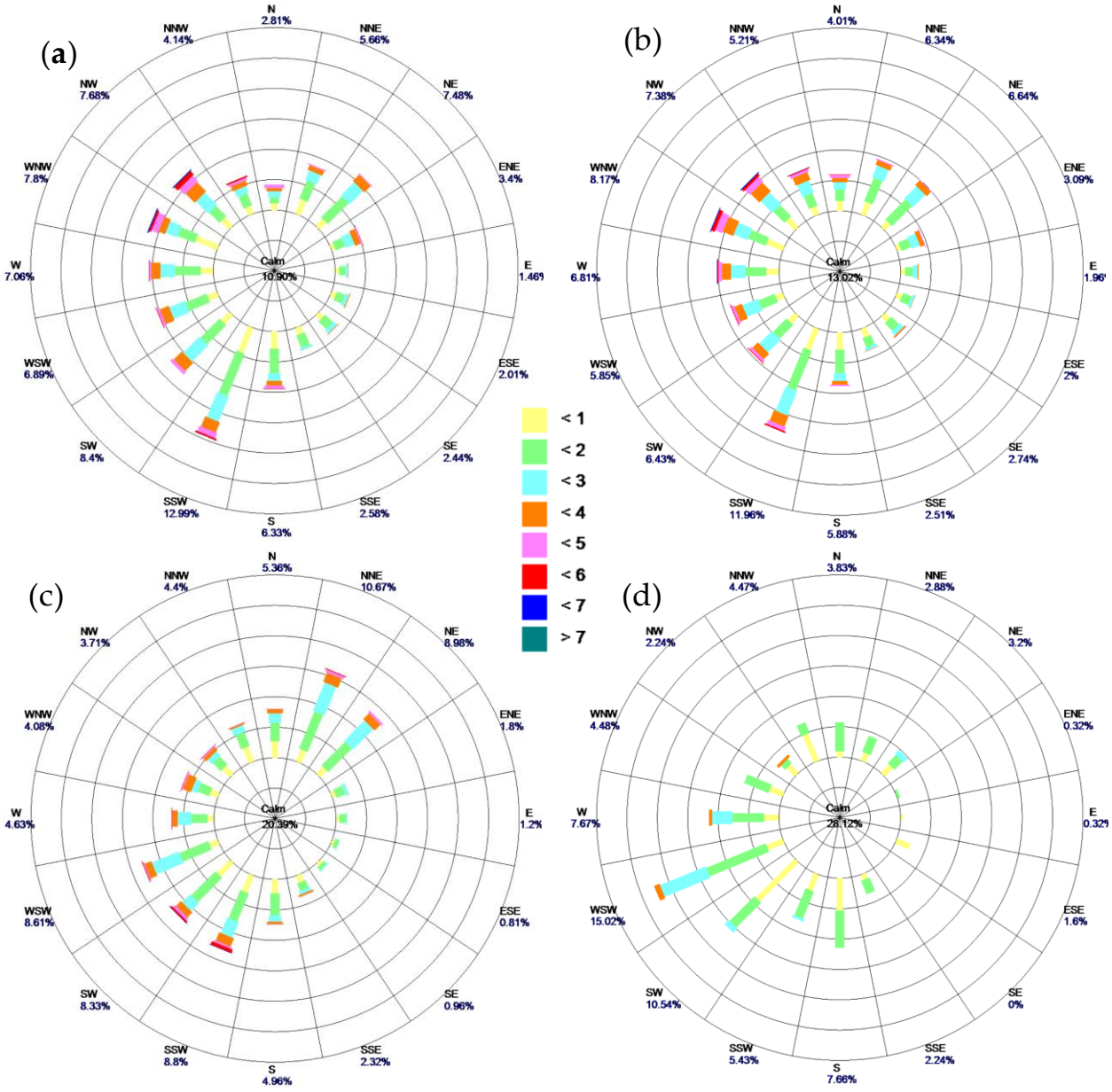

Figure SM1. Wind roses from LMAPCD monitoring stations (10 m elevation) that are closest to the project area. The Southwick monitoring station was located 1 km east of site S1, and was discontinued in February 2018, coincident with the startup of meteorological measurements at S1. The panels represent: (a) Three years of historical data from Southwick (9/12/14 - 9/12/17), (b) Southwick for the first 6 months of this project (9/12/17 - 2/6/18), (c) S1 for remainder of the first year of the project (2/6/18- 9/12/18, (d) S1 during PS period 20 (6/6/18-6/19/18) that included the SIS2 event. Figure SM1(d) indicates that site S9 (see Figure 1) was upwind of the SIS2 emissions during this PS sampling period. The color bar indicates wind speed in m/s.

Figure SM2: Comparison of field and duplicate PSs

Chromatographic calibration curves for this project were produced by diffusive loading of prepared PS tubes using a GC-monitored exposure chamber. The PS calibration tubes were exposed for 24 hours (one day) to continuous low-velocity flows of certified TO-14 gas standards that were diluted with humidified air to fixed concentration levels (calibration points). The target calibration points were: 0.0, 0.25, 0.50, 1.0, 2.0, 5.0, 25.0, and 50.0 ppbv, respectively, with the zero-point accomplished using a 0.99999 ultrapure air (VOC-free) humidified dilution exposure. This calibration approach simulated the integrated mass loadings of PSs exposed to continuous ambient pollutant mixing ratios for a 24-hour period (one exposure day), and can be expressed in units of ppbv-day. The chromatographic analysis of a field-deployed PS represents the determination of the total mass loading of a specific compound accumulated by the PS over the nominal 14-day field exposure period. For this paper, the field-deployed PS mass loadings were equated to an equivalent (theoretical) average concentration experienced by the PS by dividing its analytically-determined value (using the derived ppbv-day calibration curves) by the exact PS field exposure time in days.

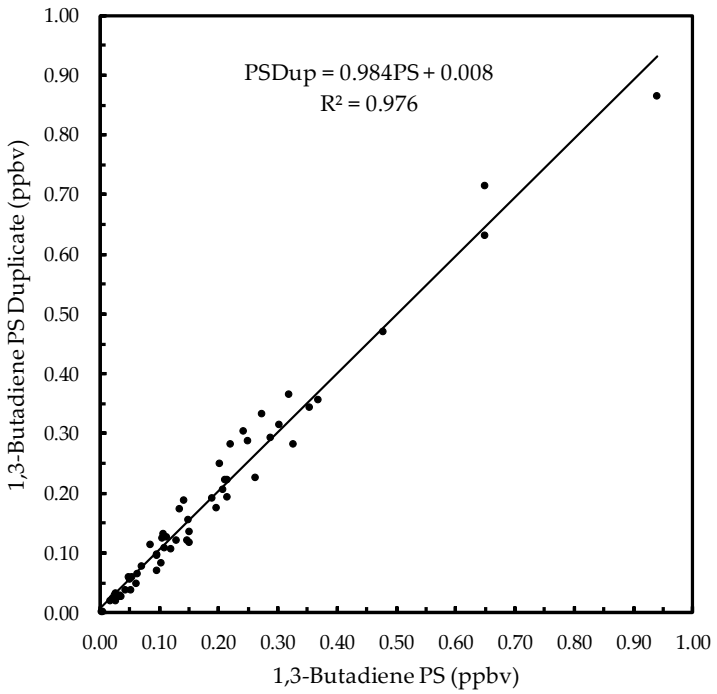

Figure SM2. Comparison of field PSs with co-deployed duplicates from 9/12/17 to 9/12/18, (N=57).

As on ongoing quality assurance measure, continuous calibration check samples (CCCS) consisting of nominal 2.0 ppbv-day PS calibration tubes were analyzed along with the field samples. For 1,3-butadiene, a total of 67 CCCS samples produced an overall mean [σ] percent recovery of 95% [σ= 11%], where percent recovery is the measured concentration divided by theoretical diffusive loading concentrations x 100). Lab spikes (N=21) and field spikes (N=26) were also prepared at nominal 2.0 ppbv-day concentrations, and exhibited recoveries of 96% [σ= 11%] and 95% [σ= 12%] respectively for 1,3-butadiene. Since the prepared PS sorbent material can carry low-level residual mass loading for some compounds, analytical values were

calculated using calibration curves that were background-corrected by subtracting the average of the zero calibration point areas from each calibration point. To achieve maximum accuracy for analysis of field samples, the calibration curves were range-selected to apply the correction most appropriate for the encountered tube loading.

In this project, a total of 321 PS field results yielding 57 duplicate pairs passed quality assurance (QA) checks, and are part of this analysis (two samples were removed for QA reasons). Duplicate pair comparisons for 1,3-butadiene exhibit strong correlation ($R2 > 0.98$, Figure SM2). Excluding 2 duplicate pair comparisons, with both values below the average method detection limit (MDL) of 0.01 ppbv, the mean, median and maximum relative percent difference of the pairs was 13.9%, 13.7%, and 30.5%, respectively. The mean, median and maximum absolute difference of the entire set of duplicate pairs (N=57) was 0.019 ppbv, 0.01ppbv, and 0.075 ppbv, respectively. Expressed on nominal 14-day exposure time basis (i.e. dividing by actual exposure days), the 1,3-butadiene residual blank correction was on average 0.016 ppbv (0.078 max), and the average MDL was 0.010 ppbv (0.027 ppbv max).

The deployment of two-week PSs for 1,3-butadiene measurements in communities is a modification of EPA Method 325 (non-benzene, non-facility fenceline application) and all factors affecting accuracy and overall method uncertainty are not fully known. Several factors that can affect a PS's ability to accurately represent average ambient pollutant concentrations are (including but not limited to): Contamination of the PS by a non-ambient source, obstructions to PS inlet during sampling (e.g. insect nest), extremely heavy rain events in windy conditions that may leave water residue on an inlet, potential variations in PS uptake rate (e.g. sorbent batch variation), the potential for back diffusion, the PS's ability to fully capture high plume gradients (proximate plumes), compound-specific issues and analysis (e.g. high blank correction values), and general uncertainties in expressing the measured PS two-week average ppbv equivalent value in ug/m3 units at actual conditions. For these reasons, absolute comparisons to low-level bench mark ambient concentrations (BACs) carries significant uncertainly.

Table SM2: Summary of 1,3-butadiene PS results.

Sampling Period Number	Period Mid-point	All Sites Mean (ppbv)	All Sites Min. (ppbv)	Loc. of Period Min.	All Sites Max (ppbv)	Loc. of Period Max.	Group S5, S7, S8 Mean	Group S4, S6, S9 Mean
1	09/20/17	0.07	0.05	9	0.11	8	0.09	0.05
2	10/04/17	0.00	0.00	3,9	0.03	10	0.00	0.00
3	10/18/17	0.14	0.04	9	0.27	8	0.23	0.10
4	11/01/17	0.08	0.03	4	0.17	10	0.09	0.03
5	11/14/17	0.16	0.07	6	0.34	5	0.27	0.08
6	11/28/17	0.24	0.09	9	0.47	8	0.41	0.16
7	12/13/17	0.12	0.01	9	0.30	8	0.23	0.03
8	12/27/17	0.07	0.03	4	0.14	8	0.12	0.04
9	01/10/18	0.07	0.02	9	0.31	5	0.14	0.03
10	01/24/18	0.12	0.02	9	0.20	8	0.17	0.04
11	02/07/18	0.09	0.00	7	0.34	10	0.10	0.03
12	02/21/18	0.18	0.02	4	1.18	1	0.10	0.03
13	03/08/18	0.35	0.02	4	1.40	5	0.90	0.05
14	03/22/18	0.08	0.02	4	0.23	2	0.09	0.05
15	04/05/18	0.14	0.04	9	0.36	8	0.25	0.04
16	04/18/18	0.10	0.01	4	0.27	8	0.21	0.05
17	05/02/18	0.11	0.02	9	0.21	2	0.14	0.05
18	05/16/18	0.17	0.05	9	0.29	8	0.25	0.06
19	05/30/18	0.32	0.13	6	0.64	8	0.45	0.19
20	06/12/18	0.39	0.02	9	0.76	5	0.71	0.31
21	06/26/18	0.11	0.04	9	0.25	7	0.18	0.07
22	07/10/18	0.11	0.03	9	0.32	8	0.25	0.05
23	07/24/18	0.10	0.02	3	0.23	8	0.19	0.05
24	08/08/18	0.21	0.05	9	0.35	8	0.34	0.11
25	08/22/18	0.09	0.02	9	0.18	3	0.10	0.05
26	09/05/18	0.09	0.00	2	0.26	10	0.11	0.06
Average	**N/A**	**0.14**	**0.03**	**N/A**	**0.37**	**N/A**	**0.24**	**0.07**
Median	**N/A**	**0.11**	**0.02**	**N/A**	**0.28**	**N/A**	**0.18**	**0.05**
StdDev.	**N/A**	**0.09**	**0.03**	**N/A**	**0.31**	**N/A**	**0.20**	**0.06**
Minimum	**N/A**	**0.00**	**0.00**	**N/A**	**0.03**	**N/A**	**0.00**	**0.00**
Maximum	**N/A**	**0.39**	**0.13**	**N/A**	**1.40**	**N/A**	**0.90**	**0.31**

Table SM2. Summary of 1,3-butadiene PS results from 9/12/17 to 9/12/18, (N=264). Field sample and duplicates are averaged. Statistics shown are calculated from values in the table, rounded to two decimal places.

Figure SM3: 1,3-butadiene results by distance and site

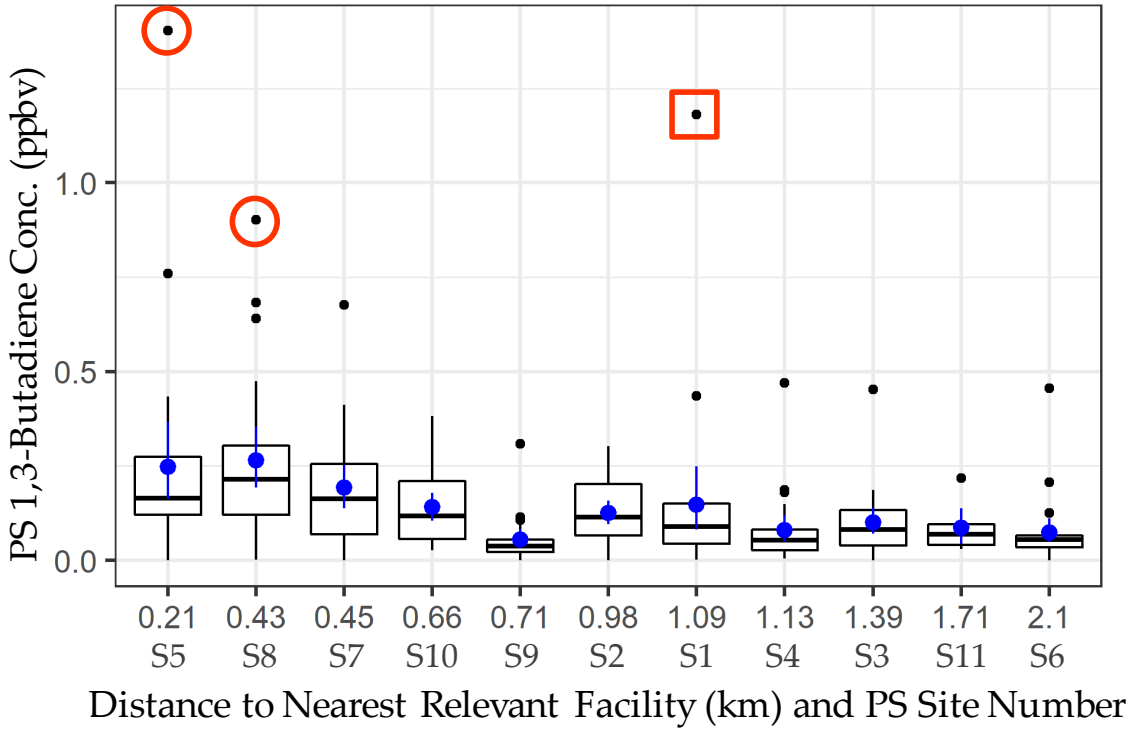

Figure SM3. 1,3-butadiene results by distance and site. The distance to the nearest relevant site is an estimate, and represents a measure from the sampling locations of Figure 1 to the approximate center of the nearest facility that works with the compound 1,3-butadiene, primarily east of S5, S7, and S8. The box whiskers extend to the largest measurement, <1.5 times the interquartile range. Blue markers indicate means with 95% confidence intervals calculated by non-parametric bootstrap. As in Figure 3, the red box and circles indicate the highest reading at S1 during period 12 and highest readings at S5 and S8 during period 13, with the former associated with SIS1.

Figure SM4: Comparison of S1 SPod and S1 10m wind data for SIS1 event

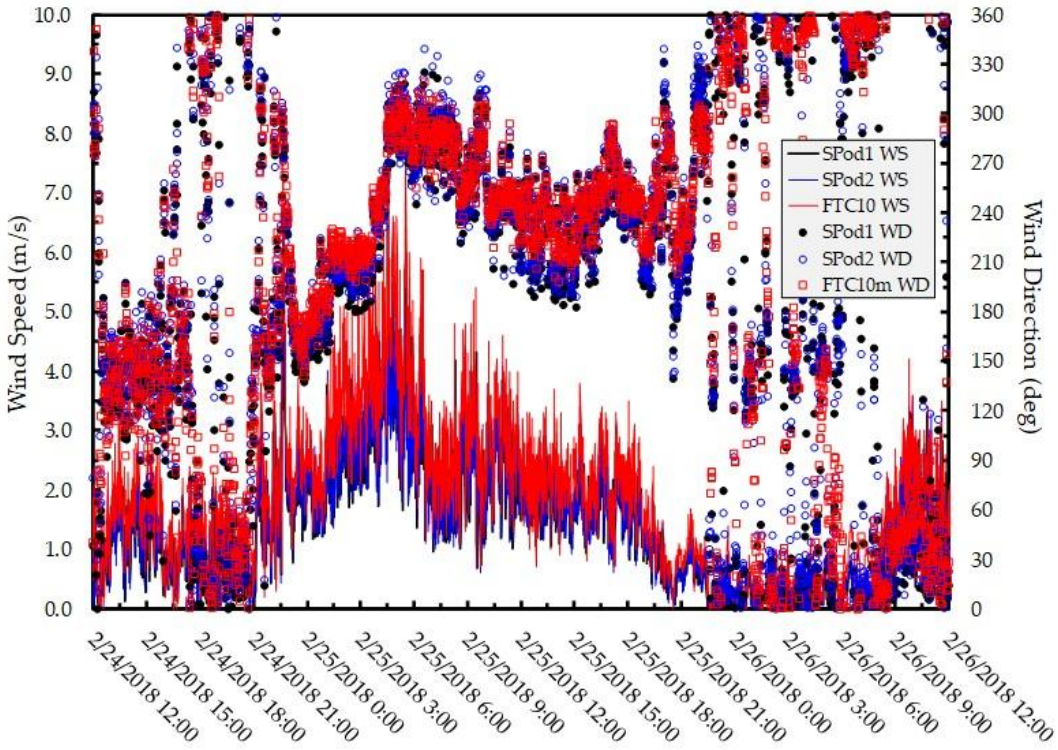

Figure SM4. Comparison of one-minute average wind speed (WS) and wind direction (WD) data from instruments deployed at S1 for the example SIS1 period described in Section 3.2. The two SPod FSs were fitted with 3-D sonic anemometers (see text for model), produced native 1 Hz data, and were deployed at 3.5 m above ground level (AGL), attached to the roof deck hand rail of the LMAPCD FTC monitoring site shelter (Figure 2a). The FTC10m data was from a 2-D sonic anemometer, (PN 86000, R.M. Young, Inc., Traverse City, MI, USA) anemometer, producing native one-minute averages deployed at 10 m AGL (Figure 2a). Elevated 1,3-butadiene concentrations were observed during the early evening of 2/24/18 and from 24:00 on 2/25/18 to 9:00 on 2/26/18 when winds were from the N (360°) and NE (~45°, Figure 5a). No 1,3-butadiene signal was observed on 2/25/18 with higher wind speeds form the W and NW.

Figure SM5: Ten second time-resolution S1 SPod wind data for SIS1 event

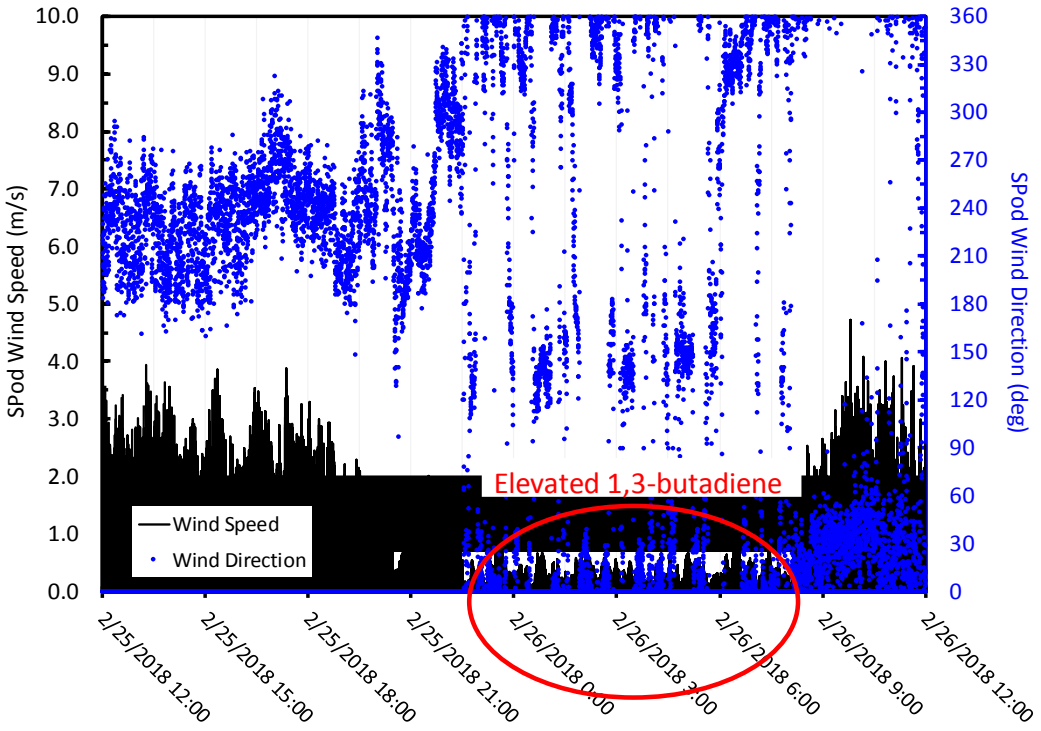

Figure SM5. Ten second time-resolution wind speed and wind direction data from SPod1 from 12:00 on 2/25/18 to 12:00 on 2/26/18, covering the period of highest recorded 1,3-butadinene concentrations at S1 (Figure 4). The elevated concentrations occurred during very low average wind speed conditions (calms) from 23:00 on 2/25/18 to 8:00 on 2/26/18, indicated by the red oval. Elevated signal at S1 occurred during wind puffs (≈0.5m/s) from N, NE. It is believed that emissions pooled at the source, and then were transported to S1 (reference Figure SM7 and Videos SM1,SM2, and SM3).

Figure SM6: Example and description of EnviroSuite BTM

In brief, the prototype version of the EnviroSuite BTM used in this paper employs a kinematic Lagrangian approach[1], based in part on D'Abreton et al. [2,3], to determine the evolving three dimensional position [P(x,y,z)] of a finite element of air (a parcel or particle) in a multi-kilometer domain with a spatiotemporally-resolved wind field V(P,t). The motion of a parcel along a path is called its trajectory, and is discussed here as being projected backwards in time (back trajectory) from observation location (e.g. sensors at S1), but could also be performed forward in time from a source location if desired. At progressive time steps, the new position of a parcel is calculated by explicit integration;

$$P(t + dt) = P(t) + V[P(t)]dt \qquad \text{Eq. 1}$$

The wind field V[P(t)] consists of the sum of a mean component $V_m[P(t)]$ and a random component that is caused by atmospheric turbulence, V'[P(t)];

$$V[P(t)] = V_m[P(t)] + V'[P(t)] \qquad \text{Eq. 2}$$

The mean component is obtained from a gridded three-dimensional wind field using the CALMET model [4,5], interpolated to produce u, v, and w wind components at the location P(x,y,z) of a parcel for each time step. For this project, a 25 km by 27 km domain was set up, with a SW corner located at 38.08788, -85.97377. The Grid spacing was 150 m. Meteorological data input from project sites S1, S8, and two other sites in the eastern part of the domain (Wave 3 News and the University of Louisville). For this exploratory work, the CALMET and back trajectory model was operated at five-minute time resolution using one-minute average wind data from the primary sites, S1 and S8 (June 19 example only). The S1 wind measurements were at 10 m above ground level (AGL), whereas the S8 measurements were at 2.3 m AGL, a typical height for a fenceline sensor system. The impact of sub 15-minute model runs and low AGL measurements are the subject of future work.

Parameterization of the turbulent component of the wind field V'[P(t)], [or V'(t)] follows the approach of Hanna et al. [6], with the term expressed as the sum of a correlated and a random component (V''');

$$V'(t)=V'(t-\Delta t)R(\Delta t)+V''' \qquad \text{Eq. 3}$$

Where the Lagrangian variable R(Δt) is:

$$R_u(\Delta t) = \exp^{-\left(\frac{\Delta t}{TLu}\right)} \qquad \text{Eq. 4}$$

with the same expression for the v and w wind components and TL, the Lagrangian time scale. As per Hanna et al., the random component V''' assumes a zero-mean Gaussian distribution, with variance defined as;

$$\sigma^2 V''' = \sigma^2 V'[1-R^2(\Delta t)] \qquad \text{Eq. 5}$$

For stable, unstable and neutral atmospheric conditions, the turbulent energy (σ^2V) is estimated from the standard deviations of the turbulent velocity fluctuations (σ_u, σ_v, and σ_w) in the x, y, and z directions [6, 7] with the Lagrangian turbulence time scales Ta_{le}, TL_v and TL_w back-calculated using a proprietary approach similar to Stohl et al. [8]. Additionally, the BTM accounts for the effect of mixing height on vertical

movement of the trajectory. The three-dimensional interpolated u, v, and w components of the mean and turbulent flow are used to determine the new parcel position at each location/time step.

Each parcel position is then compared to the 2-dimensional interpolated mixing height at each parcel location. If the parcel is higher than the mixing height at that location, it will be reflected downward from the mixing height. Further details on the EnviroSuite approach, and factors affecting performance will be provided in future work.

The prototype five-minute time resolution EnviroSuite BTM is illustrated through examples in Figure SM6, depicting individual back trajectory runs for t = 0 times of 6:40 AM and 8:50 AM on 6/19/18, respectively, associated with the discussion of SIS2 in the text. Following the blue trajectories to the SW show the position of the parcels back in time towards the t = -60 minute position, at the lower edge of frame in Figures SM6a and SM6c.

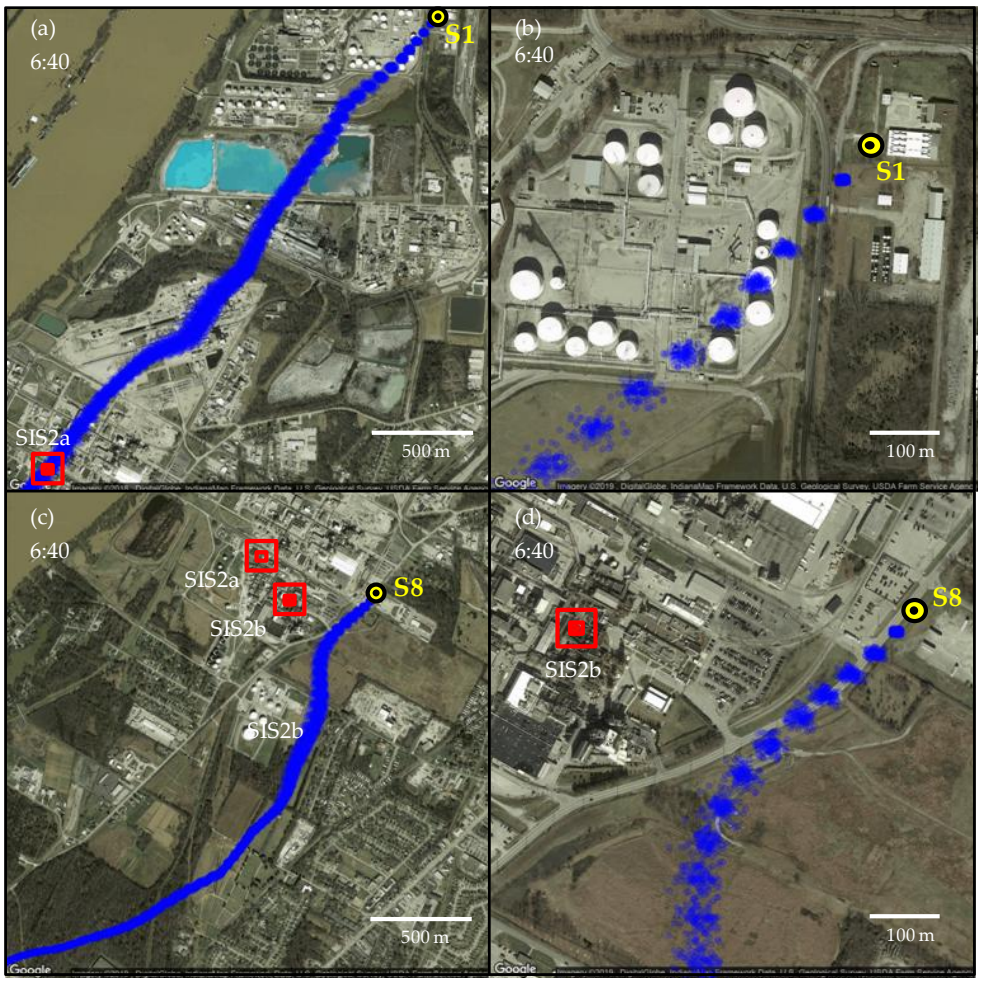

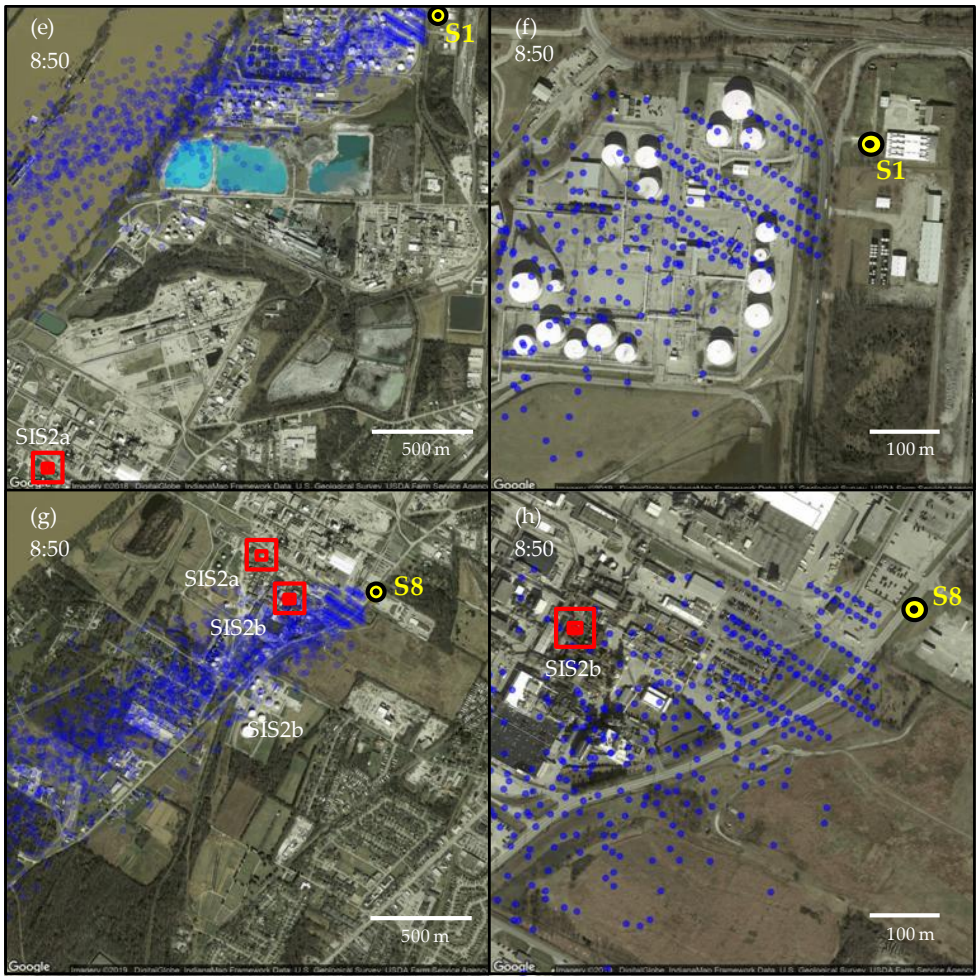

Figure SM6. BTMs for 6:40 (a-d) and 8:50 (e-h) on 6/19/18. For 6:40: (a) Multi-kilometer view from S1, (b) zoomed-in view near S1, (c) multi-kilometer view from S8, (d) zoomed-in view near S8. For 8:40: (e) Multi-kilometer view from S1, (f) zoomed-in view of near S1, (g) multi-kilometer view from S8, (h) zoomed-in view near S8.

Each model run consists of 99 calculated individual trajectories that differ from each other due to the turbulent component of the wind field in Eq. 2. In Figure SM6a, the overlap with the possible location of SIS2a is discussed in text. In Figures SM6b and SM6d, the discrete nature of the one-minute time steps is seen, as well as the slight dispersion of back trajectory points under early morning stable atmospheric conditions. Figure SM6c shows the change to a more westerly wind direction beginning to propagate into the area of interest.

In general, the dispersion in trajectories under stable atmospheric conditions appears minimal, and likely exhibits a more optimistic certainty in mean trajectory path than actual. This is because the model is not accounting for uncertainty-associated progressive wind direction meandering, among other factors. Excluding treatment of wind flow around near-field structures (see QUIC discussion), a general increase in uncertainty of the mean trajectory moving away from the T=0 position would be expected with the increase likely to be a function of atmospheric state, topographical complexity and wind field sensor data quality, proximity and node density. In Figures SM6e through SM6h at 8:40, wind speed has significantly increased (Figure SM11), and atmospheric conditions have transitioned to more unstable conditions.

As a result, the BTMs markedly changed, reflecting significantly more uncertainty with individual model runs failing to execute in some cases. The mean winds with more of a westerly component are properly represented, and the partial overlap with the potential SIS2b source location is evident but difficult to robustly quantify.

It is noted that the standard operational scheme of the CALMET/EnviroSuite trajectory model is based on 15-minute time resolution and yields and average trajectory with a measure of uncertainty. For this project, EnviroSuite produced higher time-resolution model runs using low AGL wind data in some cases, and provided the underlying trajectory information to the project team for further analysis (an exploratory approach). For these reasons, the current discussion does not necessarily reflect the performance of the model under standard operation. As noted in the text, the EnviroSuite trajectory model does not currently account for wind flow around obstructions, such as the buildings and structures, but variations of the approach are being considered, and may be explored with data from this project. Regarding model certainty under specific atmospheric states, future work may explore the direct use of wind turbulence measurements provided by 3-D sonic anemometers located at S1 and S8 in an attempt to improve model performance.

Figure SM7: Example of TCTA for 2/25/18 to 2/26/18 SIS1 event

The temporally combined trajectory analysis (TCTA) is an exploratory source location tool in development by the EPA. In TCTA, an "acceptance circle" is defined with a given radius at a suspected or potential source location, and a time series of BTM runs from the monitoring location is produced and compared with measured NGEM sensor data. For this paper, S1S1 used a 10 m or 20 m diameter acceptance circle (small diameter due to proximity to observation point) and SIS2a and SIS2b used a 50 m diameter circle. For a given period (e.g. 4:00 on 2/24/28 to 9:00 on 2/26/18 for SIS1), all possible five-minute BTM runs are executed representing a range of wind directions over the multi-hour or multi-day period. For this work the EnviroSuite BTM is used, but other similar models are being explored. For each five-minute model run, all 99 back trajectories (that execute successfully through the EnviroSuite model) were investigated using a program written in "R" (https://www.r-project.org/ *last accessed 3/20/19*) to determine the number of back trajectory points (blue data points in Figure SM6) that land inside of the defined acceptance circle for each five-minute model period. This time-resolved TCTA source location intersection count can then be compared against measured concentrations at the monitoring location with correlations providing confidence in the identification of the source location. Iterative calculation schemes to optimize the source location can be envisioned. The TCTA is rudimentary at present with issues in discrete point (one-minute time step) overlap of proximate sources under some conditions (Figures SM6a and SM6c). Temporal intermittency of the source emission will affect the analysis, as will the performance (uncertainty) of the utilized inverse model under changing atmospheric conditions (Figure SM6). The current form of the TCTA approach is illustrated in Figure SM7 and subsequent discussion with further details provided in future publications.

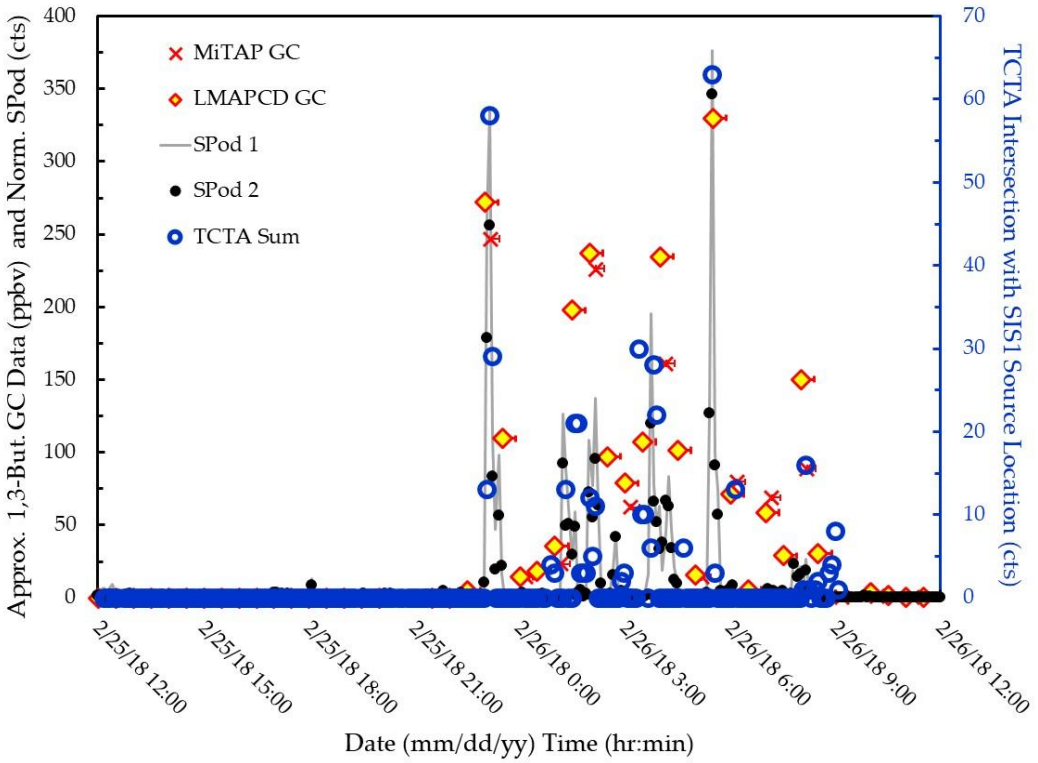

Figure SM7. Example of prototype TCTA for February 2018 SIS1 event. Time-resolved data for 2/25/18 and 2/26/18, similar to Figure 4, are shown, but with the SPod data plotted on the primary ordinate axis along with GC data (SPod counts rescaled by dividing 9 and 12 respectively). The secondary ordinate shows the TCTA intersection count reflecting the summation of all back-trajectory points (blue dots in Figure 5 and Figure SM6) landing within a 10 m radius circle around the optimized SIS1 location.

Video SM1: TCTA video for beginning of 2/25/18 SIS1 event

This video is contained in a separate file named "Video_SM1.mp4", and illustrates the sequence of five-minute BTM runs from 21:30 to 23:55 on 2/25/18 before and after the first spike in 1,3-butadiene concentration at 23:05 on 2/25/18 (reference Figure SM7). The general location of the SIS1 is represented by a star in this video. This analysis does not account for obstructed wind flow. Buildings near S1 (Figure SM8) that did play a role in observed event were investigated using the QUIC model (Video SM2).

Figure SM8: View of S1 showing structures affecting plume transport

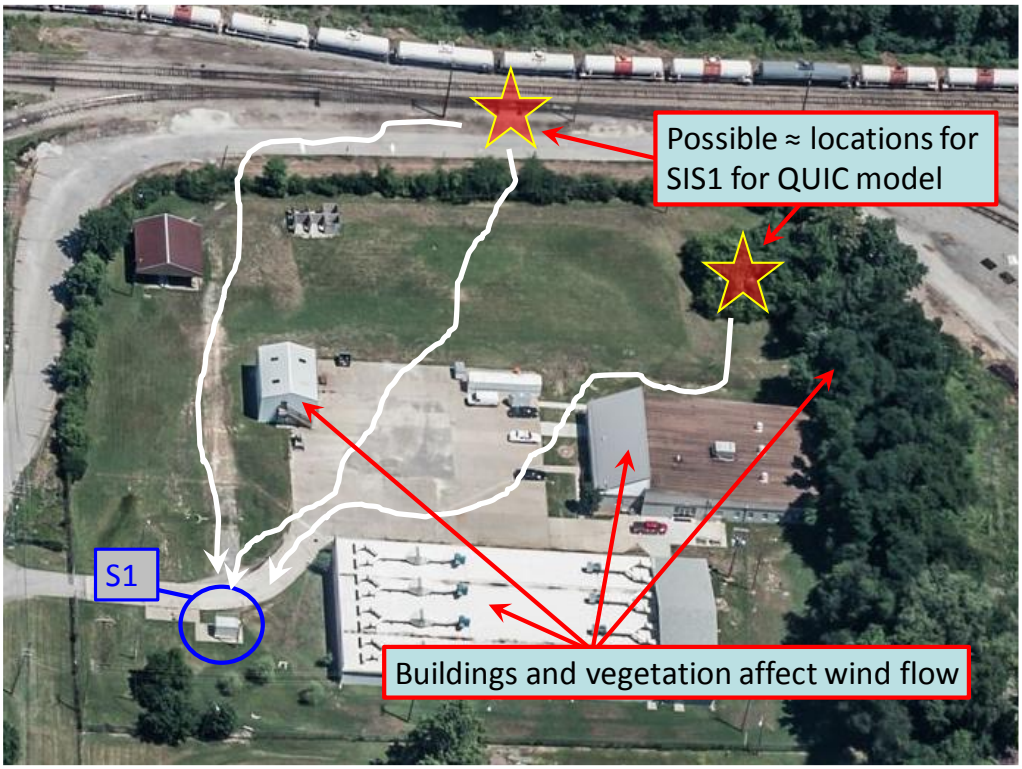

Figure SM8. Overhead view of the S1 monitoring site and nearby buildings and structures that can affect flow to the monitors with two potential source sites used in the QUIC model indicated by stars. This view shows summertime vegetation levels.

Video SM2: QUIC model video for beginning of February SIS1 event

The video is contained in a separate file with the file name "Video_SM2.mp4", and illustrates the effects of wind flow obstructions (buildings and vegetation) using the Los Alamos Quick Urban & Industrial Complex (QUIC) Dispersion Modeling System (SM reference 9). The video begins with a view of the QUIC layout showing the modeled structures, the position of monitoring site S1, and two potential locations for SIS1. The second part of the video shows the modeled results for 1.5 hours of event SIS1, including the first spike in concentration. Due to channeled wind flow by buildings near the site, it is difficult to pinpoint the location of the source. SIS1 could be located anywhere in the general area, including to the north of the railroad tracks.

Figure SM9: SDI plots for February and May 2018 SIS1 events

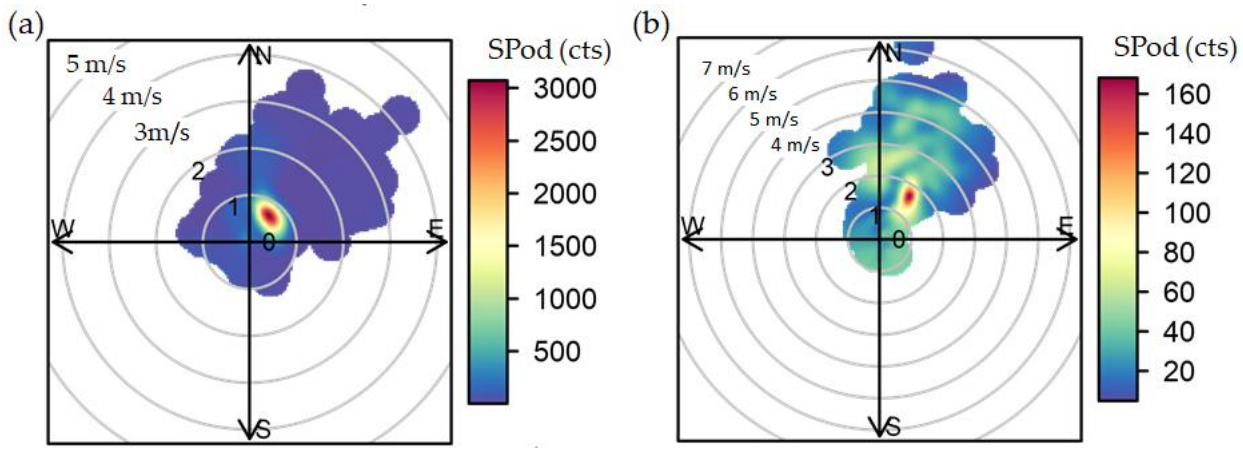

Figure SM9. S1 SPod SDI plot using 10 m wind data for (a) 23:00 2/25/18 to 11:00 2/26/18, and (b) 0:00 to 12:00 on 5/7/18, with SIS1 to the NE. Concentric circles represent WS in m/s and color bars show baseline-corrected SPod PID signal in counts. This figure illustrates that the source locations on these days were similar.

Figure SM10: Example of TCTA for 5/7/18 SIS1 event

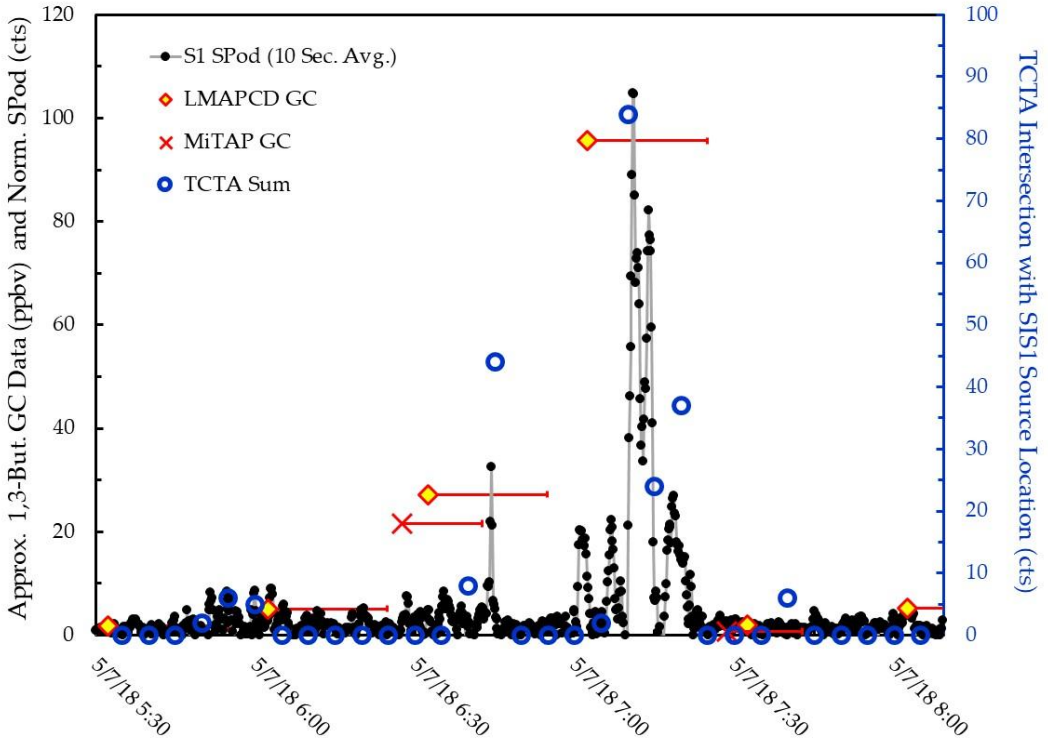

Figure SM10. Similar TCTA plot Figure SM7 showing second occurrence of SIS1 event observed on 5/7/18. Here the SPod data are shown as a 10-second average, as opposed to a five-minute average in Figure SM7. Due to the 15-minute sampling widow of the MiTAP, this GC did not record the peak near 7:15.

Video SM3: TCTA video for 5/7/18 SIS1 event

This video is contained as a separate file "Video_SM3.mp4", and illustrates the sequence of five-minute BTM runs from 5:30 to 8:00 on 5/7/18 showing the brief second occurrence of SIS1. The general location of the SIS1 is represented by a star in this video. This analysis does not account for obstructed wind flow. Buildings near S1 (Figure SM8) that did play a role in observed event were investigated using the QUIC model (Video SM2).

Figure SM11. Comparison of S8 SPod and S1 10m wind data for SIS2 event

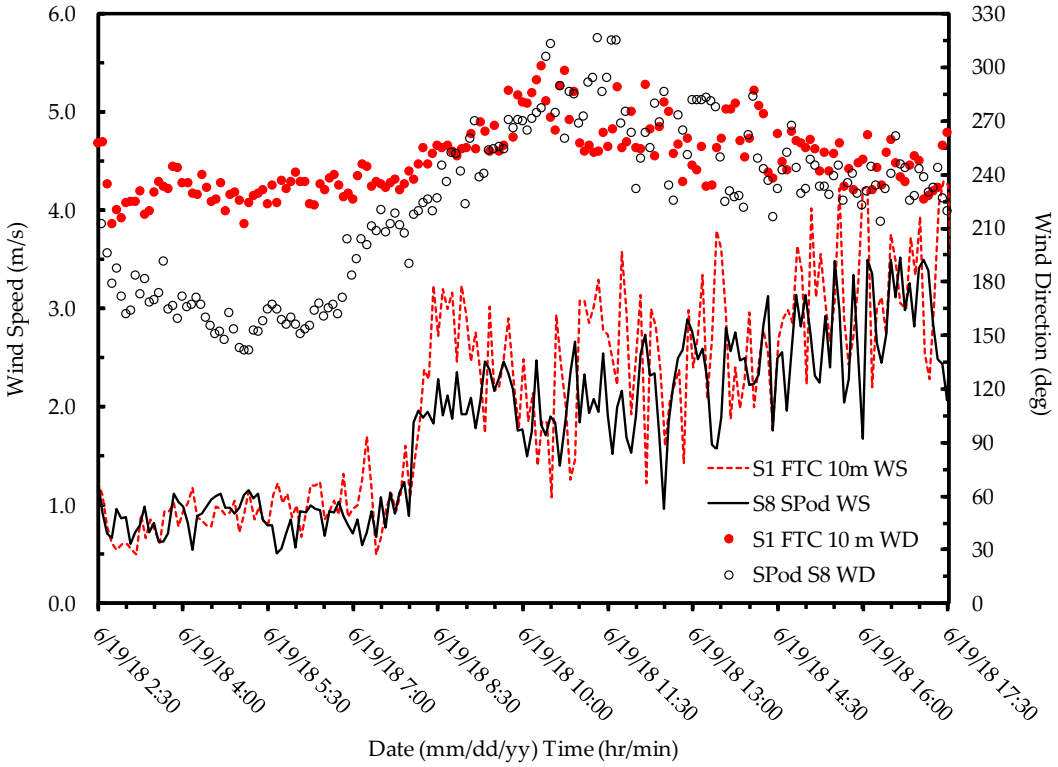

Figure SM11. Comparison of S8 SPod (2.5 m AGL) and S1 10 m AGL wind data for SIS2 event observed at S1 on 6/19/18. As indicated in Figure 6, observed 1,3-butadiene concentrations decreased at S1 and increased at S8 around 8:30 on 6/19/18, coincident with the general change in wind direction and wind speed.

Video SM4: TCTA video for 6/19/18 SIS2 event from S1.

This video is contained as a separate file "Video_SM4.mp4" and illustrates the sequence of five-minute back BTM runs originating at S1 from 4:00 6/19/18 to 10:00 on 6/19/18 during and after the observed elevated 1,3-butadiene concentrations shown in Figure 6. Signal at S1 decreases as the wind begins to move to westerly around 8:30. This analysis does not account for obstructed wind flow from structures around S1. The transition to unstable atmospheric condition (higher model uncertainty illustrated in Figure SM6) can be observed the in the latter part of the video. TCTA from S1 implies two sources may be present in the facility (SIS2a and SIS2b). This possibility of two sources cannot be confirmed based on the current analysis, as it is thought that the BTM accuracy at 3 km for stable conditions is overestimated (reference Figure SM6). The trajectories are limited to one hour back in time, and the wind speed was too low for the first few modeled trajectories to include the facility location.

Figure SM12: Example of TCTA for 6/19/18 SIS2 event from S1

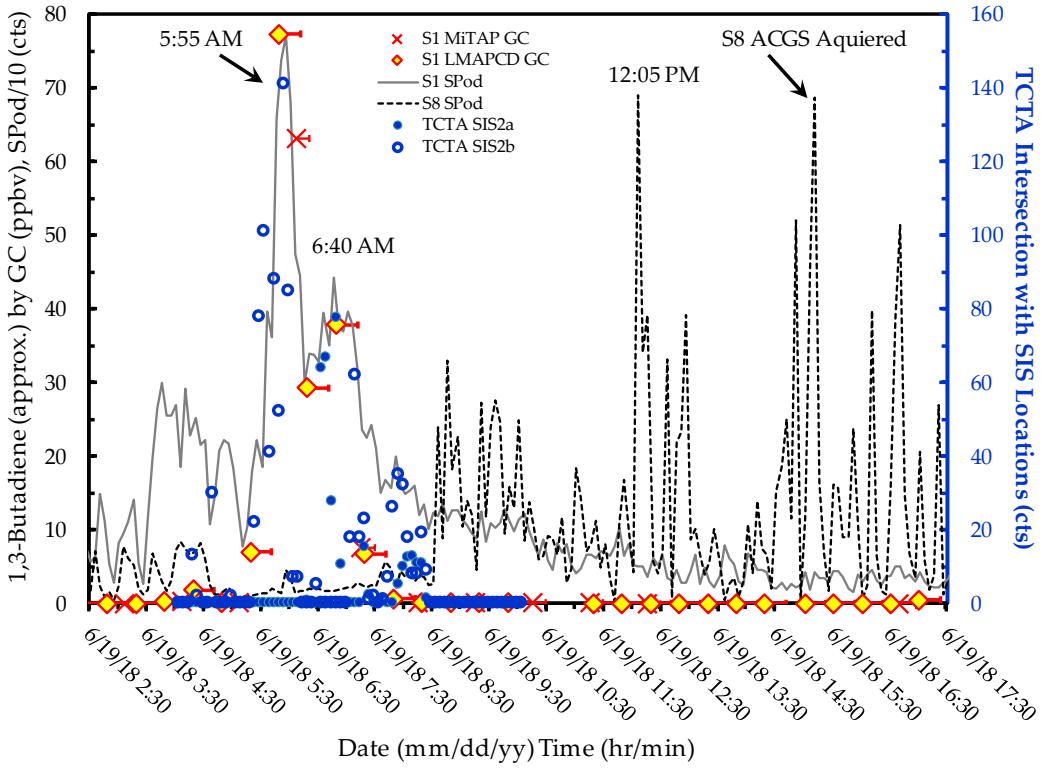

SFig. 12. Example of prototype TCTA for potential SIS2 event on 6/19/18. Time-resolved data similar to Figure 6 are shown, but with the S1 and S8 SPod data plotted on the primary ordinate axis along with GC data (SPod counts rescaled by dividing 10). The secondary ordinate shows the TCTA intersection count originating from S1 (corresponding to the trajectories shown in Video SM4), reflecting the summation of all back-trajectory points (blue dots Figure SM6 and Figure 7) landing within 50 m radius circles around the tentatively assigned SIS2a (closed circle points) and SIS2b (open circle points) locations. TCTA from S8 is not modeled due to a higher uncertainty in the back-trajectory model under unstable atmospheric conditions (Figure SM6, Video SM4). Here the TCTA SIS2a counts are divided by 2.5 for viewing purposes. The TCTA normalization is arbitrary at present, and this divisor compensates for the higher density (lower dispersion) overlap of the specific transects interesting SIS2a (reference Video SM4).

Video SM5: QUIC model video for SIS2a and SIS2b' on 6/19/18

The QUIC model video is contained as a separate file with the file name "Video_SM5.mp4", and it illustrates the two potential sources SIS2a and SIS2b' corresponding to the time period of Figure 8. Here the source terms are considered equal, are invariant in time (constant emission) and are modeled at constant atmospheric conditions corresponding to Pasquill Stability Class C (slightly unstable).

Figure SM13: QUIC model of SIS2a and non-optimized location SIS2b

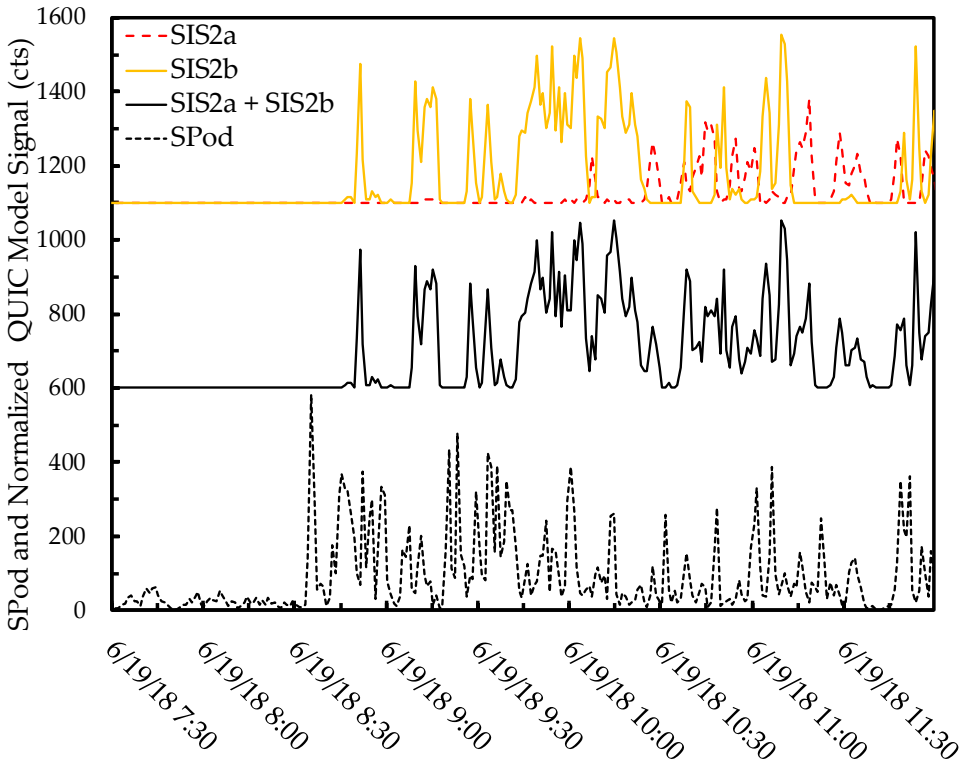

Figure SM13. Comparison of one-minute time average SPod readings from S8 (bottom panel) with QUIC model simulated emission time series from SIS2a (red dashed trace top panel), non-optimized source location SIS2b (blue trace top panel), and composite result of SIS2a and SIS2b (middle panel), with the traces offset for ease of viewing. Here the level of agreement between the composite result and the SPod-measured signal is not as good as that shown in Figure 8 in the text that uses the somewhat more optimized location SIS2b', sited 100 m directly south of the original location SIS2b (Figure 7e). In these comparisons, no correction for the transit time of the plume from the modeled source locations to the SPod sensor at S8 has been made. This distance-dependent offset is temporally variable due to wind speed changes and would improve the alignment of the initial peaks in both Figure 8 and Figure SM13. It is noted that neither of the modeled locations (SIS2b or SIS2b') reasonably reproduce the largest excursions in S8 SPod signal later in the day (Figure 6 and Figure SM12), and this may be due to a combination of non-optimal source location/obstruction definition, lack of representation of puff flow, unstable atmospheric conditions and/or temporally variable source term (south strength variable increasing). This type of optimization is explored in future publications.

References for Supplementary Materials:

1. Lin, John, Dominik Brunner, Christoph Gerbig, Andreas Stohl, Ashok Luhar, and Peter Webley, eds. Lagrangian modeling of the atmosphere. Vol. 200. John Wiley & Sons, 2013.
2. D'Abreton P.C. (1996). Lagrangian kinematic and isentropic trajectory models for aerosol and trace gas transport studies in southern Africa. S. Afr. Jour. Sci. 92, 157-160.
3. D'Abreton P.C. and Tyson P.D. (1996). Three-dimensional kinematic modelling of water vapor transport over southern Africa. Water SA, 22, 297-306.
4. Scire, Joseph S., Francoise R. Robe, Mark E. Fernau, and Robert J. Yamartino. "A user's guide for the CALMET Meteorological Model." Earth Tech, USA 37 (2000).
5. Cox, Robert M., John Sontowski, and Catherine M. Dougherty. "An evaluation of three diagnostic wind models (CALMET, MCSCIPUF, and SWIFT) with wind data from the Dipole Pride 26 field experiments." Meteorological applications 12, no. 4 (2005): 329-341.
6. Hanna, S.R., Briggs, G.A, and Hosker, R.P. (1982) Handbook on Atmospheric Diffusion, Prepared for the Office of Health and Environmental Research, Office of Energy Research, U.S. Department of Energy.
7. Panofsky, H. A., Tennekes, H., Lenschow, D. H. and Wyngaard, J. C. (1977) The Characteristics of Turbulent Velocity Components in the Surface Layer Under Convective Conditions, Boundary Layer Meteorology, 11: 355-361.
8. Stohl, A., Forster, C., Frank, A., Seibert, P. and Wotawa, G. (2005) Technical note: The Lagrangian particle dispersion model FLEXPART version 6.2, Atmospheric Chemistry and Physics, 5, 2461–2474.
9. Williams, Michael D., Michael J. Brown, Balwinder Singh, and David Boswell. "QUIC-PLUME theory guide." Los Alamos National Laboratory (2004): 43.